Civil Engineering Beyond Limits 1 (2026) 11094
Civil Engineering Beyond Limits
journal home: www.acapublishing.com/journals/1/cebel
Research Article

Numerical Investigation of the Flexural Behavior of RC Beams Strengthened with Polyurea-Coated Glass Textile-Reinforced Mortar

Birkan Simsek*,[1], Abdussamet Arslan[2]
[1]*Gazi University, Graduate School of Natural and Applied Sciences, 06500, Ankara, Türkiye*
[2]*Gazi University, Faculty of Engineering, Department of Civil Engineering, 06570, Ankara, Türkiye*

Keywords

Polyurea coating,
Finite Element Analysis,
Beam Flexural Behavior,
Textile-Reinforced Mortar (TRM),
Reinforced Concrete Beam Strengthening.

Abstract

This study numerically examines the flexural behavior of reinforced concrete beams retrofitted using a hybrid system comprising textile-reinforced mortar (TRM) and polyurea coating through finite element analysis. Nine beam models were generated in ABAQUS to analyze how strengthening levels influence stiffness, crack control, load capacity, and ductility parameters. Numerical results indicated that one TRM layer with polyurea coating enhances peak load by nearly 150–180%, while two TRM layers achieve an increase of about 200-270%, depending on the concrete strength used. The initial stiffness for strengthened beams also improves significantly to nearly 2–3 times that of unstrengthened models. This study is purely numerical and has not been calibrated with any experimental program; hence results should be interpreted in this light. All interfaces (steel-concrete, concrete-TRM, and TRM-polyurea) were modeled using perfect bond assumptions (embedded + tie), representing an upper-bound strengthening response without slip or debonding. Under these idealized conditions, the hybrid TRM-polyurea system provides consistent improvements in crack confinement, peak load, stiffness, and deformation stability for all levels of concrete strength.

1. Introduction

Most of the buildings in earthquake-prone areas, particularly those near active fault lines, were not built according to today's design standards or recent seismic regulations. The main reasons for this are weak concrete, poor details in the reinforcement, and construction methods without proper engineering control. These buildings could seriously endanger life and property under possible earthquake forces, so it is important to improve their performance. Since new buildings are expensive, take a lot of time to build, and are limited by environmental factors, the best choice is to upgrade existing ones because it is cheaper and better for the environment. In this situation, creating and using good upgrading methods is a key engineering duty to guarantee safety in structures.

Textile-reinforced mortar (TRM) composites have emerged as one of the most efficient techniques for strengthening and rehabilitating reinforced concrete (RC) members in recent years. High-strength textile fabrics—usually in the form of meshes or woven grids—are integrated into a mineral-based mortar matrix to form TRM composites. These systems, due to their material properties, offer substantial benefits such as enhanced bond and compatibility with concrete and masonry substrates, permeability for moisture transfer, and better performance at high temperatures and fire exposure [3, 4]. Because of these properties, TRM systems have become a practical alternative to conventional strengthening techniques and are being increasingly used in various structural rehabilitation applications.

The tensile behavior of TRM systems exhibits a very complex mechanism due to their multi-component and heterogeneous nature. The load-carrying process starts with the cracking of the mortar matrix, after which most of the tensile stress is transferred and carried by the textile reinforcement. This sequential stress transfer mechanism creates a nonlinear response with multiple cracking stages on the stress–strain curve. The different slope changes in the curve are controlled by both the post-cracking behavior of the matrix and the deformation capacity of the textile reinforcement. Hence, the total mechanical performance of the system is governed by interaction among matrix, textile reinforcement, and interface as well as material property effects from each component working together [5, 6].

In TRM systems, the high ultimate strains coming from direct tensile tests conducted only on the bare textile fabric under laboratory conditions are often not fully mobilized within the composite system. When applied to reinforced concrete elements, TRM presents that the interface between the mortar matrix and the textile reinforcement becomes the weakest part in terms of structural behavior. It is because of this weak interface that bond degradation happens within the matrix–textile interaction zone before reaching maximum deformation capacity in textile reinforcement; thus, premature debonding failures take place. As a result, the system will show earlier-than-expected tensile rupture or just a slight increase in load-carrying capacity. This makes it clear that interface behavior in TRM systems is an important factor controlling their total mechanical performance [7, 8].

The debonding in TRM systems has been a significant topic of interest in recent years. D'Ambrisi and Focacci [9] examined the influence of different textile and matrix types on interface behavior, demonstrating the critical role of material combinations in governing the debonding mechanism. Ombres [10] reported that systems incorporating high-strength textiles tend to exhibit premature failure modes originating from the interface. Elsanadedy et al. [11] showed that U-shaped textile configurations enhance interface adhesion and improve the load-transfer capacity of the system. Similarly, Raoof et al. [12] found that surface coating of the textile increases interface strength and debonding stress.

*Corresponding Author: birkan.simsek@gazi.edu.tr
Received 02 Dec 2025; Revised 04 Dec 2025; Accepted 04 Dec 2025
https://doi.org/10.36937/cebel.2026.11094

The pre-tensioning technique proposed by Park et al. [13] improved interface performance by ensuring proper alignment and positioning of the textile during application. Giese et al. [14] systematically investigated the effects of parameters such as the number of textile layers, mortar age, and material properties on the debonding process. Al-Saidy et al. [15] reported that the use of ready-mix repair mortars and distributed U-anchor details enhances the ductility of the system. Finally, Kirthiga and Elavenil [16] observed that employing fiber-reinforced mortars leads to textile rupture rather than debonding, resulting in a more balanced and stable structural response. Collectively, these studies demonstrate that the debonding mechanism is not governed solely by the adhesive properties of the binding matrix, but is also strongly influenced by a wide range of parameters including geometry, textile surface characteristics, application technique, and anchorage details.

Polyurea coatings have emerged as an innovative and effective alternative technique for the strengthening of reinforced concrete structural members. Greene and Myers [17] reported that discrete fiber-reinforced polyurea (DFRP) coating systems provide significant enhancements in both the flexural and shear capacities of reinforced concrete beams, while also substantially improving ductility. Similarly, Marawan et al. [18] conducted experiments on small- and large-scale beams strengthened with spray-applied polyurea coatings of various thicknesses and observed an approximate 20% increase in flexural capacity and more than a 40% increase in shear capacity. In the same year, Parniani and Toutanji [19] demonstrated that polyurea coatings are effective not only under static loading but also under cyclic (fatigue) loading; they reported that a 5-mm-thick coating enhanced the flexural capacity by 17.4% and maintained fatigue resistance up to two million cycles. Supporting these findings, Song and Eun [20] showed that glass fiber-reinforced polyurea (GFRPU) systems exhibit particularly high performance in terms of shear behavior, achieving nearly a tenfold increase in ductility compared to control beams. More recently, Yu et al. [21] investigated a hybrid system combining polyurea with glass fiber-reinforced polymer (GFRP) fabric, reporting stronger adhesion and more effective flexural strengthening compared to traditional epoxy-based methods.

This study presents a hybrid strengthening system that combines the complementary benefits of TRM and polyurea coatings to eliminate the drawbacks associated with using each of these systems separately. TRM enhances flexural stiffness in RC members by inhibiting crack initiation and delaying crack propagation, while polyurea possesses high ductility, excellent adhesion, and large energy-dissipation capacity under significant deformations. Although both systems have been previously used successfully for strengthening applications, their joint use as a hybrid solution has not received much attention in research, indicating an existing gap in the literature on possible performance enhancement through such a combination, particularly concerning RC beams.

A numerical analysis was conducted in the ABAQUS 6.14 software to fill this gap. The models created are used to study the flexural performance of RC beams strengthened with a TRM–polyurea hybrid system and to examine how variations in concrete compressive strength, the number of TRM layers, and textile arrangement influence the overall response of the beams. More specifically, it examines how hybrid systems influence stiffness evolution, cracking patterns, ultimate load capacity, and their dependence on material properties and strengthening levels. Additionally, this study aims to determine the upper-bound structural performance that could be achieved under the assumption of perfect bond conditions at all interfaces.

2. Material Properties

In the numerical models, three different concrete strength levels (10.5, 18.5, and 22.5 MPa) and a single grade of steel rebar (B420C) were used. The material properties of concrete and steel rebar are presented in Table 1.

Table 1. Material properties of reinforcement and concrete

Concrete (MPa)			Steel Rebar		
			Ø (mm)	f_y (MPa)	f_u (MPa)
10.5	18.5	22.5	8	490	604

The hybrid strengthening system used in this study consists of three components: the mortar and GFRP textile employed in the TRM layer, and the polyurea coating. The mortar exhibits a compressive strength of approximately 5 MPa and a tensile strength of around 1 MPa. It has moderate elasticity and excellent bond properties. The GFRP reinforcement, while having a relatively low ultimate strain capacity, provides high stiffness with an elastic modulus of 72 GPa and a tensile strength of 1350 MPa. Polyurea, on the other hand, is intended to impart significant ductility to the structural system, with a tensile strength of 25 MPa and an ultimate elongation of roughly 350%. The material properties of the strengthening components are presented in Table 2.

Table 2. Material properties of strengthening components

GFRP Fabric	Tensile Strength of GFRP Mesh (kN/m)	125
	Areal Weight (g/m²)	590
	Elastic Modulus (GPa)	72
	Tensile Strength (MPa)	1350
	Ultimate Strain	0.0187
	Specific Gravity (g/cm³)	2.68
Polyurea	Tensile Strength (MPa)	25
	Tear Strength (MPa)	96
	Elongation at Break (%)	350
Mortar	Density (kg/m³)	1500
	Flexural Strength (MPa)	≥2
	Compressive Strength (MPa)	≥6

3. Finite Element Analysis

The nonlinear finite element analysis of the models was carried out using the ABAQUS software.

3.1. Concrete

The material parameters of concrete in this study were derived from selected compressive strength values, empirical equations, design codes, and numerical studies found in the literature [22-24]. The concrete was modeled as nonlinear using the Concrete Damaged Plasticity (CDP) model. The CDP model describes uniaxial tensile and compressive stress–strain responses of concrete with two separate constitutive curves. Typical stress–strain relationships used to define compressive (a) and tensile (b) behavior are shown in Figure 1.

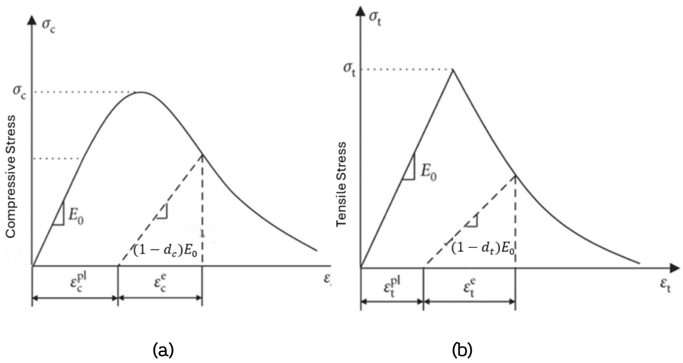

Figure 1. Compressive (a) and tensile (b) stress–strain curves of concrete

Where;
E_0: Elastic modulus (initial elastic slope), σ_c: Maximum compressive strength, σ_t: Maximum tensile strength, d_c: Compressive damage parameter, d_t: Tensile damage parameter, ε_c: Compressive strain, ε_t: Tensile strain, ε_c^{pl}: Equivalent plastic strain in compression, ε_t^{pl}: Equivalent plastic strain in tension, ε_c^{e}: Equivalent elastic strain in compression, ε_t^{e}: Equivalent elastic strain in tension.

CDP parameters used in this study are summarized in Table 3. These values were selected based on the calibration recommendations of Jankowiak and Lodygowski (2005) for concrete compressive strengths in the range of 10–25 MPa, which corresponds to the strength levels analyzed in this study [24].

Table 3. CDP Parameters

Dilation Angle	Eccentricity	fb0/fc0	K	Viscosity Parameter
35	0.1	1.16	0.667	0.0005

The compressive material behavior of concrete was defined based on the formulations proposed by Carreira and Chu [25]. This method uses parameters that have physical significance and can be identified through experiments to represent both the rising and falling parts of the stress-strain curve. The shape parameter of the curve is derived from the elastic modulus of concrete, its maximum compressive strength, and the strain value at peak stress. In this way, it is possible to describe the transition from an elastic area to a plastic domain smoothly and realistically.

For the tensile behavior, an exponential softening law was adopted to represent crack formation and the post-peak stiffness degradation. The tensile strength of concrete was defined as a function of its compressive strength, while the corresponding tensile strain was calculated based on the elastic modulus. In the numerical model, the complete tensile stress–cracking strain data and the associated tension-damage parameters used by the CDP model are summarized in Table 4. The same tension-softening curve was assigned to all three concrete grades (10.5, 18.5 and 22.5 MPa).

Table 4. Tensile stress–cracking strain and tension-damage parameters used in the CDP model

No	Tensile Stress (MPa)	Cracking Strain	Damage Parameter (dt)
1	4.0000000	0	0
2	2.8327050	0.0001766875	0.2918237
3	2.0433487	0.0003533750	0.4891628
4	1.5269940	0.0005300625	0.6182515
5	1.1944578	0.0007067500	0.7013873
6	0.9784034	0.0008834375	0.7553991
7	0.8320209	0.0010601250	0.7919974
8	0.7248911	0.0012368125	0.8187772
9	0.6385872	0.0014135000	0.8403523
10	0.5628277	0.0015901875	0.8592904
11	0.4925095	0.0017668750	0.8768726

The defined stress–strain relationships represent the nonlinear behavior of concrete under both tensile and compressive loading. The model can accurately simulate the initiation of cracks, plastic deformation, and damage build-up at the elemental level to give a realistic prediction of how the structure would behave.

3.2. Steel reinforcement

B420C reinforcing steel was used in the numerical model. The steel behavior was defined using a bilinear elastoplastic material model. The parameters related to the elastic range were as follows: Young's modulus was 210,000 MPa, and Poisson's ratio was taken to be 0.30. The yield strength of the steel was assumed to be 490 MPa, and its ultimate tensile strength was 604 MPa. Post-yielding, the stress-strain behavior followed a mild strain-hardening curve until an ultimate strain of 0.10, with a tangent hardening modulus of approximately 1,170 MPa. This bilinear idealization is consistent with TS 708 and with numerical modeling approaches commonly adopted in the literature [26]. The complete material parameters associated with the steel model are summarized in Table 5. Figure 2 shows the corresponding stress–strain relationship.

Table 5. Mechanical properties of reinforcing steel used in the bilinear elastoplastic model

Parameter	Symbol	Value
Elastic modulus (MPa)	E	210,000
Poisson’s ratio	ν	0.30
Yield strength (MPa)	fy	490
Ultimate strength (MPa)	fu	604
Yield strain	εy	0.00233
Ultimate strain	εu	0.10
Tangent hardening modulus (MPa)	Et	1,170

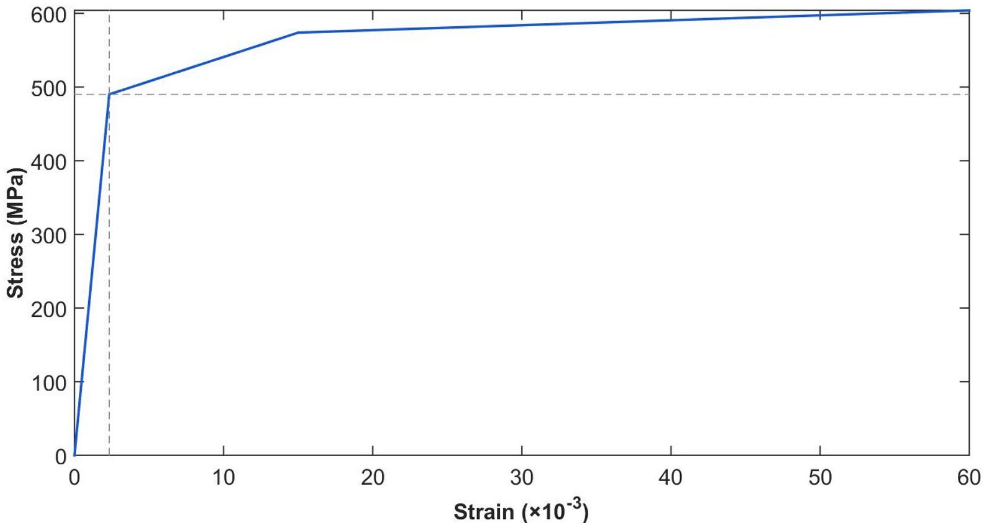

Figure 2. Stress–Strain relationship of steel rebar

3.3. TRM

The TRM layer was modeled as a two-phase composite system consisting of a cement-based mortar and a glass-fiber textile mesh. The mechanical properties of the constituent materials are presented in Table 6. Using these properties, together with experimental data reported in the relevant literature, the equivalent orthotropic elastic parameters of the TRM system were derived in the “Engineering Constants” format by applying thickness/volume-weighted mixture rules [27].

Table 6. Mechanical properties of constituent Materials

Mortar	Elastic Modulus (MPa)	7500
	Poisson’s Ratio	0.2
GFRP Fabric	Elastic Modulus in Fiber Direction (MPa)	72000
	Elastic Modulus Transverse to Fiber Direction (MPa)	5000
	Shear Modulus in Fiber Direction (MPa)	28000
	Shear Modulus Transverse to Fiber Direction (MPa)	2200
	Poisson’s Ratio	0.22

The equivalent elastic modulus in the fiber direction, the transverse elastic modulus, the Poisson's ratio in the fiber direction, the shear modulus along the fiber direction, the shear modulus transverse to the fibers, and the equivalent density were calculated using Equations (1)–(7), respectively. Since the elastic behavior of the TRM layer represents a composite action between the fibers and the mortar matrix, a single equivalent Poisson's ratio was adopted in the modeling rather than assigning separate Poisson's ratios to the individual components. This value was selected based on the ranges recommended in the literature for similar TRM systems [28].

$$V_f = \frac{t_f}{t_m + t_f} \tag{1}$$

$$E_1 = V_f E_{f1} + (1 - V_f)E_m \tag{2}$$

$$\frac{1}{E_2} = \frac{V_f}{E_{f2}} + \frac{1 - V_f}{E_m} \tag{3}$$

$$G_m = \frac{E_m}{2(1 + v_m)} \tag{4}$$

$$G_{12} = V_f G_{f12} + (1 - V_f)G_m \tag{5}$$

$$\frac{1}{G_{23}} = \frac{V_f}{G_{f23}} + \frac{1 - V_f}{G_m} \tag{6}$$

$$\rho = V_f \rho_f + (1 - V_f)\rho_m \tag{7}$$

Where;

V_f: fiber volume fraction, t_f: effective thickness of the glass fiber mesh, t_m: mortar thickness, E_1: equivalent elastic modulus in the fiber direction, E_{f1}: elastic modulus of fibers in the longitudinal direction, E_m: elastic modulus of the mortar, E_2: equivalent elastic modulus transverse to the fibers, E_{f2}: transverse elastic modulus of fibers, G_m: shear modulus of the mortar, v_m: Poisson's ratio of the mortar, G_{12}: equivalent shear modulus in the fiber direction, G_{f12}: shear modulus of fibers in the longitudinal direction, G_{23}: equivalent shear modulus transverse to the fiber direction, ρ: equivalent density, ρ_f: density of the glass fiber mesh, ρ_m: density of the mortar.

Using the above mixture-rule equations, the equivalent orthotropic elastic constants of the TRM layer were computed for both the 1-layer and 2-layer configurations. The final values implemented in the ABAQUS model are summarized in Table 7.

Table 7. Ortotropic material properties of TRM layers

Parameter	Unit	1-Layer TRM	2-Layer TRM
E1	MPa	13,200	15,734
E2	MPa	7,280	7,181
E3	MPa	7,280	7,181
ν12	–	0.22	0.22
ν13	–	0.24	0.24
ν23	–	0.22	0.22
G12	MPa	5,340	6,301
G13	MPa	3,025	2,981
G23	MPa	3,025	2,981
Mass density	kg/m³	1,536	1,551

3.4. Polyurea

In this study, the polyurea coating applied over the TRM layer was modeled as a hyperelastic material due to its high elongation capacity, low elastic modulus, and nonlinear elastomeric behavior. Since the stress–strain response of polyurea differs from that of conventional elastic–plastic materials and exhibits nonlinear energy-storage characteristics under large deformations, the Neo-Hookean hyperelastic formulation was adopted to represent its constitutive behavior. The isochoric (deviatoric) hyperelastic constant $C_{10}$and the volumetric constant D_1, which are required to define the hyperelastic model, were calculated using Equations (8) and (9) based on the nearly incompressible elastomeric nature of polyurea. The material constants used in the analysis are presented in Table 8.

$$C_{10} = \frac{E}{4(1+v)} \tag{8}$$

$$D_1 = \frac{2(1-2v)}{E} \tag{9}$$

Where;

C_{10}: isochoric (deviatoric) hyperelastic constant, E: 100% modulus, v: Poisson's ratio, D_1: volumetric hyperelastic constant.

Table 8. Material constants

C10 (MPa)	D1 (1/MPa)
16.8	0.0012

4. Structural Analysis and Modeling

4.1. Part module

In this study, a total of nine reinforced concrete beam models were developed. The models were categorized into three groups based on their strengthening configuration: unstrengthened reference beams (3 specimens), beams strengthened with TRM + polyurea containing a single layer of GFRP (represented through the equivalent material approach) (3 specimens), and beams strengthened with TRM + polyurea containing two layers of GFRP using the same equivalent material approach (3 specimens). The concrete and reinforcement details were kept identical for all models; only the equivalent mechanical properties of the TRM layer were modified according to the amount of GFRP incorporated.

The concrete beam was modeled as a single 3D deformable solid. The longitudinal reinforcement and stirrups were defined as 3D deformable wire elements. The system for strengthening included a TRM layer that was applied to three faces of the beam, with a polyurea coating laid on top of the TRM. In this research, the TRM layer has been consistently modeled geometrically as a single, continuous layer. The presence of one or two layers of GFRP within the TRM was not represented by drawing separate geometric layers; instead, it was modeled through an equivalent material approach in which the mechanical properties of the TRM were adjusted according to the amount of GFRP reinforcement. In this way, the TRM layer maintained the same thickness and geometry in all models, while its material characteristics varied depending on the model group. The polyurea coating was modeled as a 3D solid layer with uniform thickness in all strengthened specimens.

The general characteristics of the model groups are presented in Table 9. The configuration of the unstrengthened reference beam is shown in Figure 3, while a typical cross-section of the strengthening system is illustrated in Figure 4.

Table 9. General characteristics of the model groups

Group	Specimen	Concrete Strength (MPa)	Number of Textile Layers	Steel Rebar Grade	Longitudinal Reinforcement	Stirrups	Polyurea Thickness (mm)	TRM Thickness (mm)
A	A-10.5	10.5						
	Ai-10.5		1				3	16.8
	Aii-10.5		2					
B	B-18.5	18.5			Upper Bars: 2Ø8			
	Bi-18.5		1	B420C	Lower Bars: 2Ø8	Ø8/70	3	16.8
	Bii-18.5		2					
C	C-22.5	22.5						
	Ci-22.5		1				3	16.8
	Cii-22.5		2					

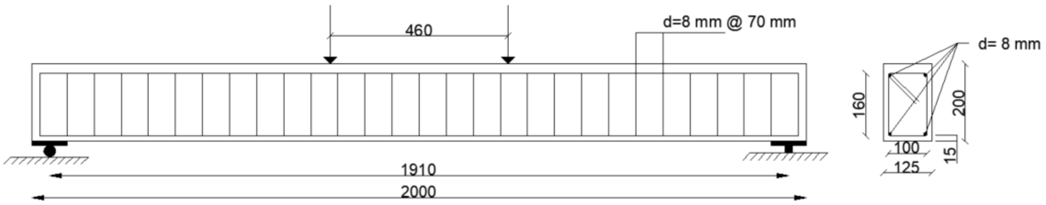

Figure 3. Reference beam

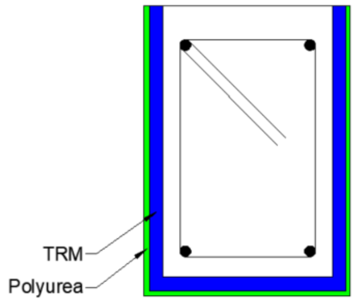

Figure 4. Hybrid strengthening system

4.2. Property module

In the analytical model, all materials were explicitly defined and assigned to the corresponding parts through section definitions. For concrete, density, elastic modulus, and Poisson's ratio were specified, after which the nonlinear behavior was introduced using the CDP model, incorporating the compressive and tensile stress–strain curves along with the associated damage parameters. For the polyurea layer, the density was defined, and its nonlinear elastomeric response was represented using the isotropic Neo-Hookean hyperelastic model, for which the C_{10} and D_1 coefficients were assigned.

For the longitudinal reinforcement and stirrups, the steel material was modeled with an elastic–plastic constitutive law; the elastic modulus, Poisson's ratio, and post-yield plastic strain characteristics were specified accordingly. The TRM layer was defined using its density and orthotropic elastic properties in the engineering constants format.

After completing all material definitions, the concrete, TRM, and polyurea components were modeled as solid sections, while the reinforcement bars and stirrups were modeled as beam sections and assigned to the corresponding geometric parts.

4.3. Assembly module

At this stage, all components created within the Part module were assembled, and the finite element configuration for each beam model was generated. The complete geometry of the strengthened beam is presented in Figure 5.

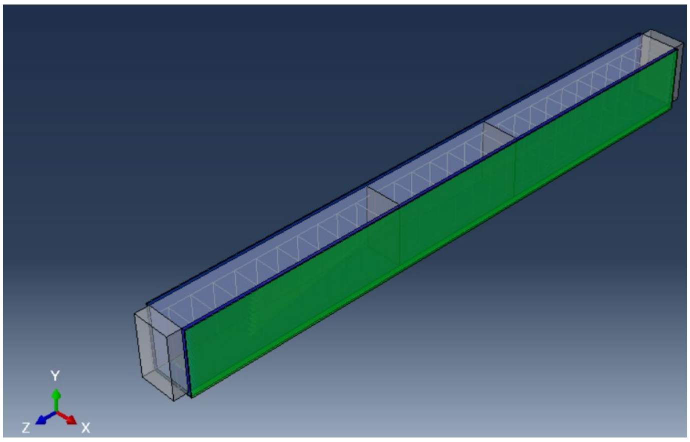

Figure 5. Strengthened beam model

4.4. Step module

To capture the nonlinear flexural behavior of the model, the analysis was conducted under a single Static, General step. In this step, geometric nonlinearity was activated so that cracking–softening effects in concrete, yielding of reinforcement, and stiffness variations within the TRM–polyurea strengthening system could be accurately represented.

To mitigate potential convergence issues arising from crack initiation in the tensile zone of concrete and material softening in the strengthening layers, the automatic stabilization technique was employed. The stabilization energy was kept very low, and an adaptive stabilization scheme was preferred to ensure that stabilization was activated only when necessary during critical increments. This approach allowed the solution to remain stable during sudden stiffness reductions associated with crack propagation.

Increment control was defined automatically within the loading step, enabling the use of smaller increments during the initial stages of the analysis and larger increments in later stages. Minimum and maximum increment limits were set to ensure stable progression of the solution, and the total number of increments was kept sufficiently high to accurately follow the full nonlinear response.

The Full Newton solution algorithm was adopted. This method updates the stiffness matrix at every increment and is therefore more suitable for tracking the nonlinear behavior arising from the concrete damage model and the TRM–polyurea composite system. For handling discontinuities within the solution, the default approach allowing data transfer between increments was retained. The load was applied using a linearly increasing scheme to ensure more controlled progression of the solution.

To monitor damage distribution, stress–strain fields, displacements, and reaction forces with high resolution, field outputs were recorded at every increment across all regions. These variables included tensile and compressive damage in concrete, stress and strain tensors, nodal displacements, and support reactions. This allowed for a detailed examination of the processes involved in crack propagation, stiffness degradation, strength development, and ultimate failure mechanisms.

The defined loading step ensured a reliable and stable nonlinear flexural analysis for all nine beam models examined in this study.

4.5. Interaction module

In this study, the interface behaviors representing the interaction among concrete, reinforcement, the TRM mortar layer, and the polyurea coating were modeled based on full-bond assumptions, which are widely used in the literature and correspond to the upper-bound (most optimistic) composite capacity of the system. The interaction between concrete and steel rebar was defined using the Embedded Region technique. This approach was adopted because explicitly modeling bond–slip behavior is highly complex, and reinforcement in laboratory-scale specimens is generally assumed to be well anchored within the concrete. Thus, an ideal connection without relative slip between steel and concrete was established.

The concrete–TRM and TRM–polyurea interfaces were modeled using Tie Constraints. This decision was based on the high initial adhesion typically observed between these layers, as well as the focus of the present study, which centers on evaluating the global effectiveness of the hybrid strengthening materials rather than capturing interface debonding mechanisms. A tie constraint enforces displacement compatibility between two surfaces with no separation or slip, representing a “perfect bond” condition.

Extensive studies on CFRP–concrete systems have shown that the perfect bond (tie) assumption does not fully reproduce the actual interface slip behavior and tends to overestimate stiffness and ultimate capacity when compared with experimental results [29]. Thus, the embedded + tie approach used in this research can be viewed as an optimistic idealization that assumes complete bonding among the concrete, TRM, and polyurea layers. This modeling strategy provides an upper-bound composite response, where interface-related damage mechanisms such as debonding, peeling, or shear slip are not explicitly simulated.

4.6. Load and boundary conditions

In the finite element model, the boundary conditions and loading configuration were defined to accurately represent the analytical behavior of a beam subjected to four-point bending. Both ends of the beam were modeled using pin-like supports in which translational degrees of freedom were restrained while rotational degrees of freedom remained free. In ABAQUS, this boundary condition was implemented by constraining all displacement components (U1, U2, U3) at the beam ends while leaving all rotational components unconstrained. Thus, the beam was idealized as a pin–pin system that is free to rotate under bending but restricted against horizontal and vertical translation.

Restricting axial displacement at the supports prevents the beam from freely elongating and shortening during loading, resulting in a limited axial stress field along the member. This condition is referred to in the literature as an axially restrained simply supported beam and is known to enhance the stability of the analytical solution by introducing secondary membrane effects in beams subjected to flexure. In the present study, controlling axial freedom contributed to improved stability in the nonlinear solution process [30].

The loading configuration was defined in accordance with the four-point bending setup by prescribing a vertical displacement at two separate loading regions on the top surface of the beam. These two loading points were positioned symmetrically, and an identical displacement amplitude curve was applied to each, ensuring that the load was introduced simultaneously and with equal magnitude. This configuration created a constant-moment region between the loading points and allowed the characteristic behavior of four-point bending to be accurately reproduced in the numerical model.

Within the Static, General step, the applied displacement was defined in a displacement-controlled manner using a ramped amplitude curve to ensure smooth transfer of load into the system. Displacement control facilitated stable tracking of concrete cracking, reinforcement yielding, and activation of the TRM–polyurea strengthening system throughout the nonlinear response.

These boundaries and loading conditions were identically applied to all nine beam models, ensuring that the only differences among the models arose from the strengthening configurations. This provided a consistent and reliable basis for comparative analyses.

4.7. Mesh generation

The finite element mesh used in the numerical model was designed to capture the complex material behavior of the reinforced concrete section and the interaction of the TRM–polyurea strengthening system with sufficient accuracy, while keeping the computational cost at a reasonable level. The same meshing strategy was applied to all models, ensuring that comparisons among different strengthening configurations depended solely on material and strengthening parameters, not on mesh-related variations.

For the concrete beam and the strengthening layers (the TRM mortar layer and the polyurea coating), C3D8R elements from the ABAQUS library were employed. These are eight-node linear brick elements with reduced integration and hourglass control. Separate but comparable global mesh seed values were assigned to the concrete, TRM, and polyurea parts, ensuring element-size compatibility among the three layers. Curvature control was activated, allowing the element size to automatically refine in regions with higher geometric gradients—particularly near the beam ends and around the loading zones. This approach provided a smoother stress field in areas where crack formation was expected and contributed to improved convergence stability.

The longitudinal reinforcement bars and stirrups were modeled as embedded line elements within the concrete volume. Two-node B31 beam elements with a shear-flexible Timoshenko formulation were used. For the longitudinal bars, a relatively coarse but uniform mesh was applied along the beam length, whereas the stirrups were discretized with a finer mesh to more accurately capture crack patterns and shear stress distribution within the cross-section. The reinforcement meshes were generated independently of the concrete solid mesh and were subsequently incorporated into the concrete using the embedded region interaction.

The TRM layer was meshed using element sizes compatible with the concrete mesh, producing near-matching nodes along the concrete–TRM interface. The polyurea coating, although relatively thin, was discretized with at least two elements through its thickness to more realistically represent its stress gradient and potential softening behavior. The C3D8R elements used for all layers help mitigate locking issues commonly encountered in nonlinear analyses and reduce computational cost due to their reduced integration scheme.

The final finite element mesh was created using the element types and global seed values chosen based on preliminary trials. The same mesh configuration was used for all beam models, so that differences in numerical results were due to different material definitions and strengthening configurations, rather than mesh variations.

5. Analysis Results and Discussion

5.1. Deformation modes

When the final crack patterns and deformation modes of the nine beams are evaluated collectively, a highly consistent trend emerges in terms of crack initiation, propagation direction, penetration depth, and the extent of the plastic hinge region. Each of the A, B, and C groups exhibits distinct behaviors depending on the level of strengthening; and a clear improvement in crack control is observed as the configuration progresses from unstrengthened beams to models strengthened with two layers of TRM + polyurea.

The damage and deformation distribution of the A-group beams is presented in Figure 6. In the unstrengthened beam, cracks initiate at early stages of loading and spread across a wide region in the mid-span. The cracks extend upward along the beam depth, and the plastic hinge region expands over a noticeably large area. In the model strengthened with a single layer of TRM from the same groups, the cracks subdivide into smaller surface segments and exhibit a more uniform distribution; the plastic hinge zone narrows, and the depth of crack penetration decreases. In the model with two TRM layers, crack widths become significantly smaller, the cracks are confined to micro-segments on the surface, and the deformation shape acquires a much more stable form.

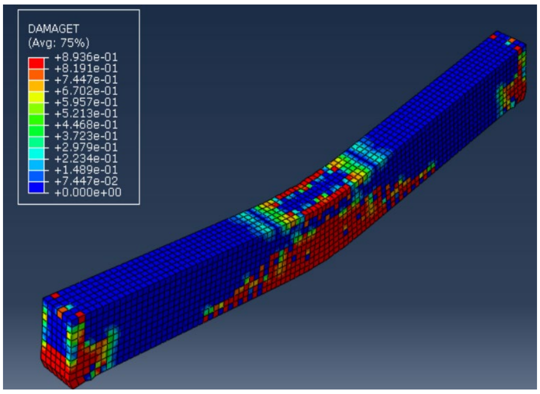

(a)

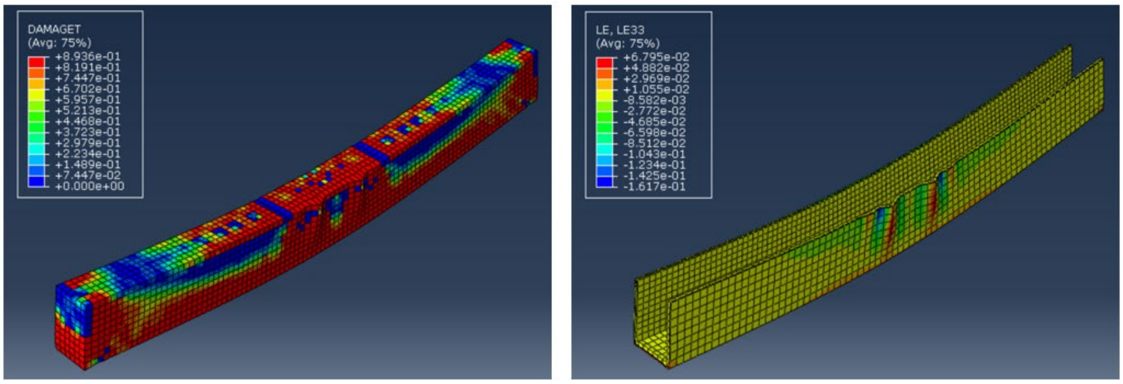

(b)

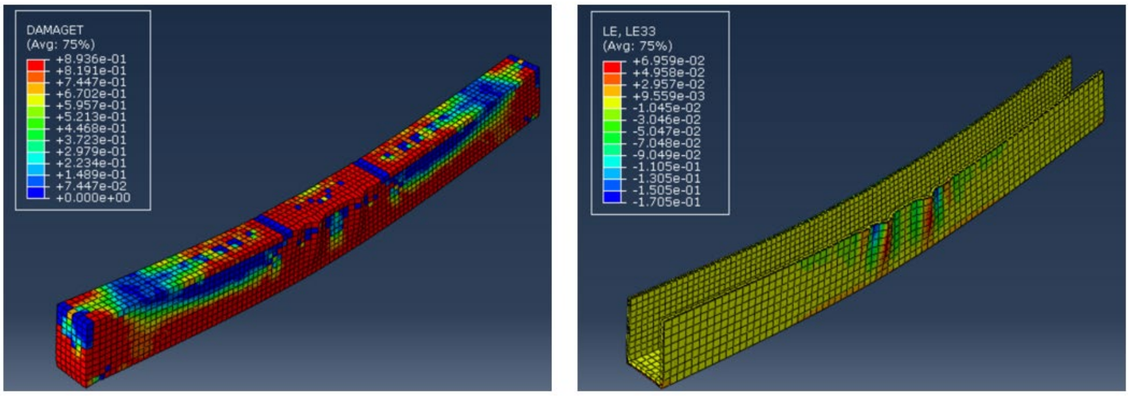

(c)

Figure 6. (a) Tensile damage in beam A-10.5; (b) Tensile damage in the reinforced concrete section and longitudinal tensile strain distribution in the strengthening layer under loading for beam Ai-10.5; (c) Tensile damage in the reinforced concrete section and longitudinal tensile strain distribution in the strengthening layer under loading for beam Aii-10.5.

The damage and deformation distribution of the B-group beams is presented in Figure 7. A similar trend is also observed in this group. In the unstrengthened beam, cracks are concentrated around the mid-span but exhibit a more limited spread compared to the A-group. In the beam strengthened with a single TRM layer, the cracks appear with smaller openings and a more uniform arrangement; the plastic hinge zone becomes confined to a narrower region. In the model strengthened with two TRM layers, the cracks are restricted to very fine surface lines, the deepening of cracks is effectively prevented, and the flexural response transforms into a significantly more stable structural behavior.

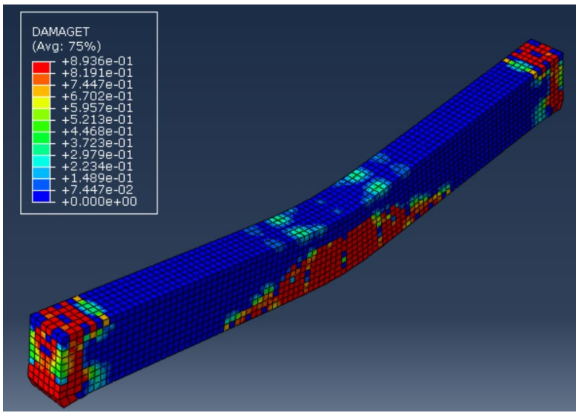

(a)

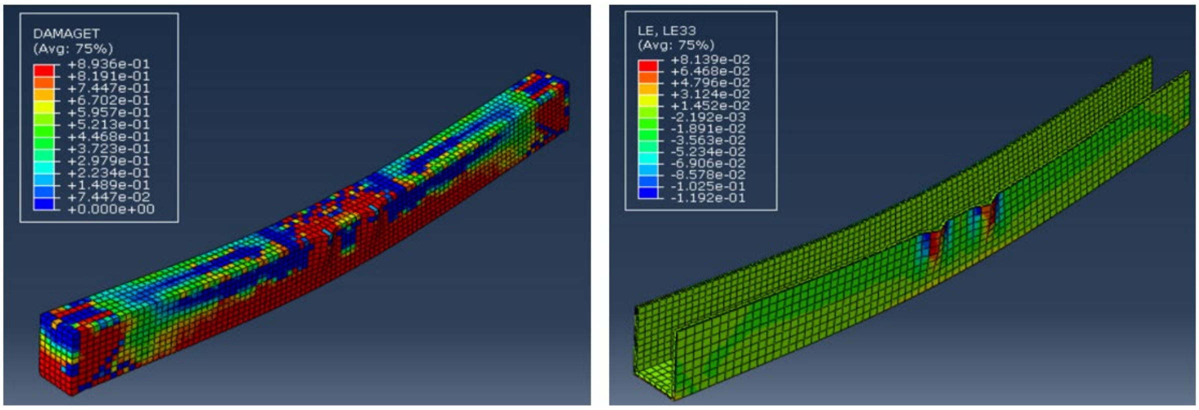

(b)

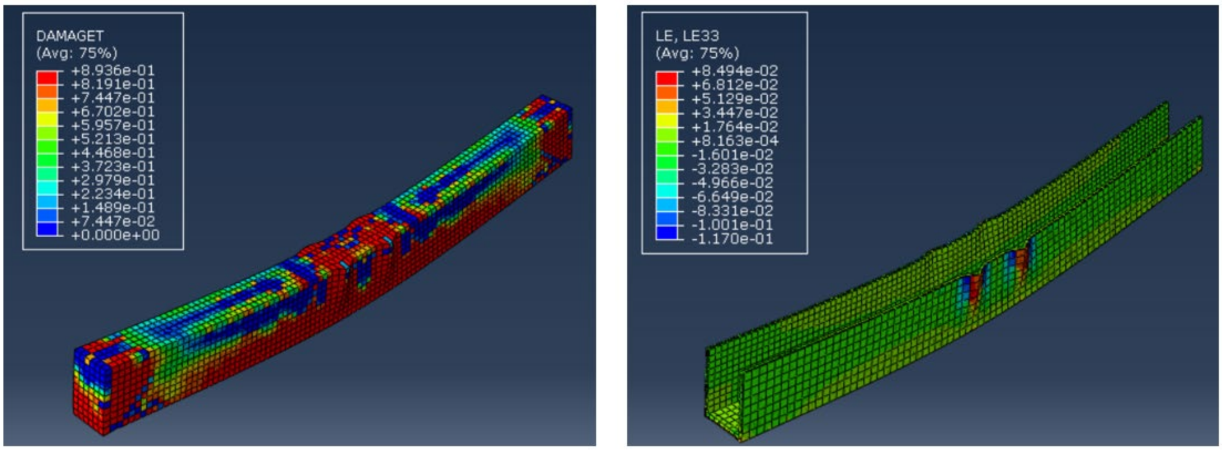

(c)

Figure 7. (a) Tensile damage in beam B-18.5; (b) Tensile damage in the reinforced concrete section and longitudinal tensile strain distribution in the strengthening layer under loading for beam Bi-18.5; (c) Tensile damage in the reinforced concrete section and longitudinal tensile strain distribution in the strengthening layer under loading for beam Bii-18.5.

The damage and deformation distribution of the C-group beams is presented in Figure 8. In the unstrengthened beam of this group, cracks appear in fewer numbers and manifest as shorter surface lines, with the plastic hinge region remaining confined to a narrow zone. In the model strengthened with a single TRM layer, the cracks further diminish in width and appear as fine surface lines concentrated near the outer regions. In the model strengthened with two TRM layers, the cracks are almost entirely confined to the surface; the plastic hinge region becomes the narrowest among all models, and crack development stabilizes in the form of micro-segments on the surface. This model exhibits the most controlled and restricted crack propagation behavior among all beams examined.

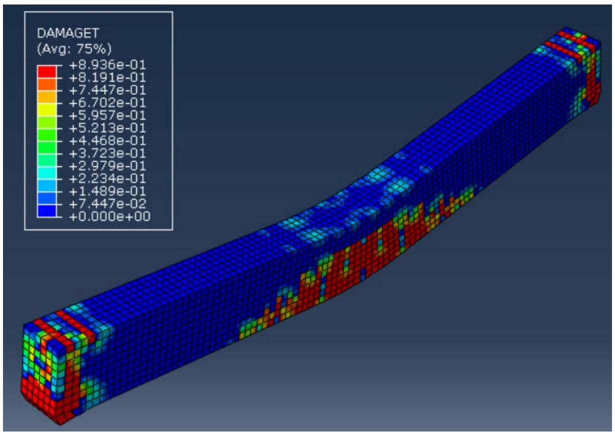

(a)

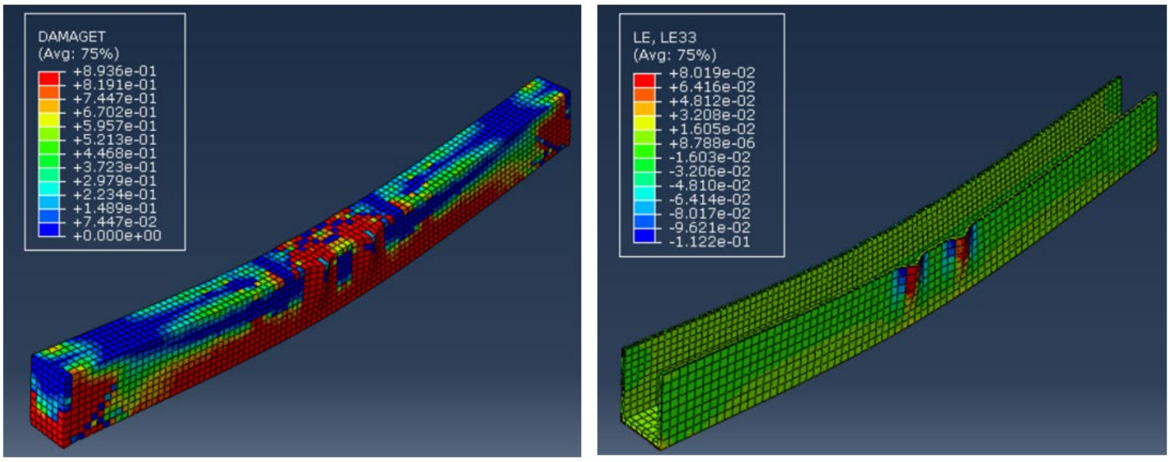

(b)

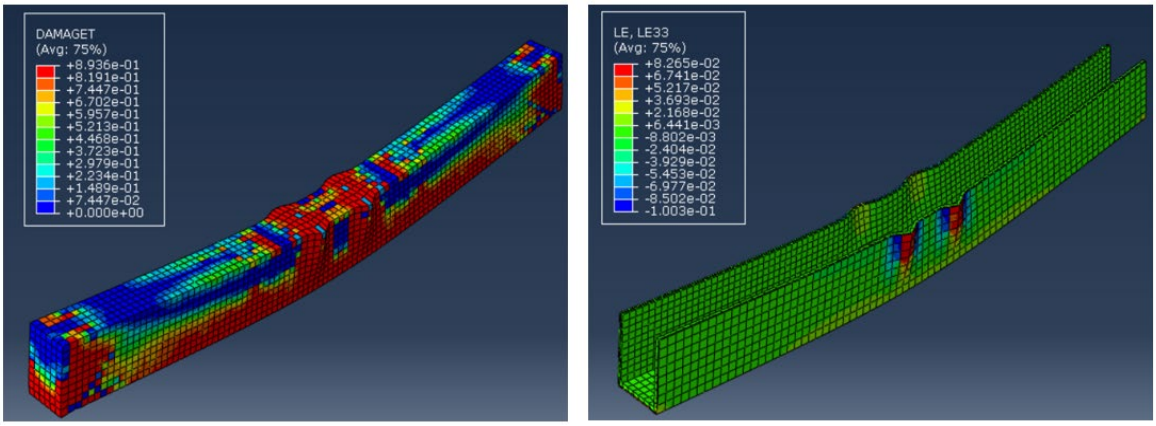

(c)

Figure 8. (a) Tensile damage in beam C-22.5; (b) Tensile damage in the reinforced concrete section and longitudinal tensile strain distribution in the strengthening layer under loading for beam Ci-22.5; (c) Tensile damage in the reinforced concrete section and longitudinal tensile strain distribution in the strengthening layer under loading for beam Cii-22.5.

5.2. Load–Deflection curves

The load–displacement curves of the A-group beams are presented comparatively in Figure 9. In the unstrengthened A-10.5 beam, a low initial stiffness is observed at the beginning of loading, followed by an early peak as the first cracks form, after which a sharp drop in capacity occurs.

The limited load-carrying capacity of approximately 6 kN and the rapid stiffness degradation indicate that the post-cracking load resistance of low-strength concrete is weak.

In the Ai-10.5 beam model strengthened with a single layer of TRM + polyurea, the initial stiffness increases substantially, the post-cracking segment of the curve progresses with a flatter trend, and the peak load reaches nearly three times that of the unstrengthened specimen. Owing to the TRM layer's ability to restrict crack propagation and the polyurea coating's deformation capacity, the response after the peak load exhibits a more gradual softening rather than an abrupt drop. This demonstrates that the strengthening system significantly enhances the flexural ductility of the beam.

In the Aii-10.5 model strengthened with two layers of TRM + polyurea, both capacity and ductility reach their highest levels. The curve displays a steeper elastic branch and attains a maximum load of approximately 21–22 kN. The nearly plateau-like behavior after the peak load indicates that the cracks are confined to micro-segments near the surface and that the plastic hinge region becomes minimal in width. Accordingly, the Aii-10.5 model exhibits the most stable and highest-performing behavior within the A-group in terms of both strength and deformation capacity.

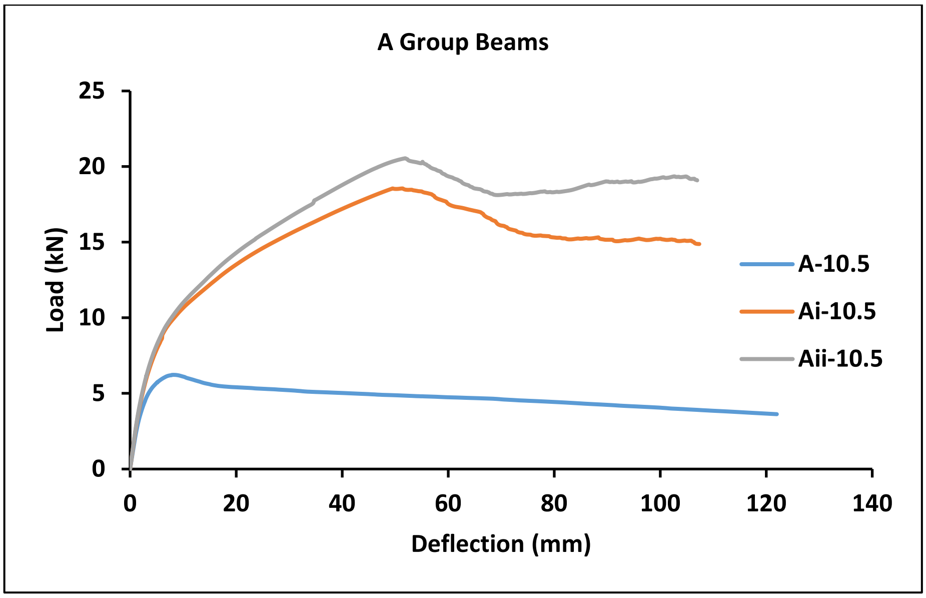

Figure 9. Load–Deflection curves of group A beams

The load–displacement curves of the B-group beams are presented comparatively in Figure 10. In the unstrengthened B-18.5 beam model, although the initial stiffness is relatively limited, the higher concrete strength compared to the A-group results in a more stable pre-cracking response, and the peak capacity reaches approximately 10 kN. After cracking, the stiffness decreases rapidly and the curve exhibits a gradual descending branch. This behavior indicates that medium-strength concrete, due to its limited crack-control capability, experiences a rapid loss of capacity following the peak load.

In the Bi-18.5 beam model strengthened with a single layer of TRM + polyurea, the initial slope of the curve increases significantly, the post-cracking region is characterized by a longer ascending branch, and the load capacity reaches approximately 26–27 kN. The single-layer strengthening application results in a more controlled surface crack distribution, leading to substantial improvements in both peak load and pre-peak stiffness compared to the unstrengthened model. The post-peak softening in this model is more gradual, indicating that the system is able to sustain its load-carrying ability for a longer duration.

The Bii-18.5 beam model strengthened with two layers of TRM + polyurea delivers the highest performance in the B-group. The steeper elastic branch of the curve demonstrates that the strengthening system significantly increases the beam's stiffness. The load capacity of approximately 30–32 kN surpasses both the B-18.5 and Bi-18.5 models. The short-term fluctuations observed in the post-cracking region may be associated with localized stress concentrations at the interface. The relatively flat behavior following the peak indicates that the two-layer TRM application effectively confines crack formation to fine surface segments and leads to the development of a more localized plastic hinge region.

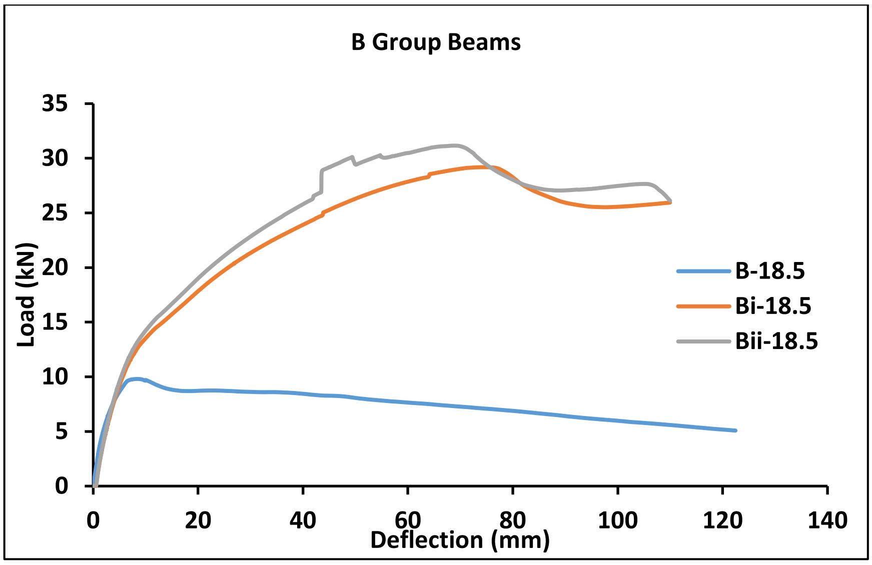

Figure 10. Load–Deflection curves of group B beams

The load–displacement curves of the C-group beams are presented comparatively in Figure 11. In the unstrengthened C-22.5 beam model, the initial stiffness is noticeably higher than that of the lower-strength groups; however, after cracking, the curve softens in a similar manner, and the load-carrying capacity remains at approximately 11–12 kN. The progressively decreasing stiffness after the peak load is associated with the limited crack-control capability of the concrete.

In the Ci-22.5 beam model strengthened with a single layer of TRM + polyurea, the elastic portion of the response becomes significantly steeper, the post-cracking segment exhibits a longer and more stable ascending trend, and the load capacity increases to approximately 29–30 kN. These findings show that the strengthening system effectively confines cracks and enables a more controlled development of the plastic hinge region. The relatively low level of post-peak softening represents a significant enhancement in the ductility of the system.

The Cii-22.5 beam model, strengthened with two layers of TRM and polyurea, exhibits the best performance among all the C-groups. The steep rise in the elastic part of the curve indicates that using two TRM layers gives the most significant increase in stiffness. Its peak capacity of about 32–33 kN is higher than that of both the C-22.5 and Ci-22.5 models, meaning that more strengthening layers directly increase the load-carrying capacity. The short-term changes observed after the maximum are due to localized stress redistributions resulting from the very close confinement of the TRM-polyurea system to microcracks at the near-surface. In this model, crack propagation is almost entirely limited to the surface, resulting in a narrow plastic hinge region and very stable flexural behavior.

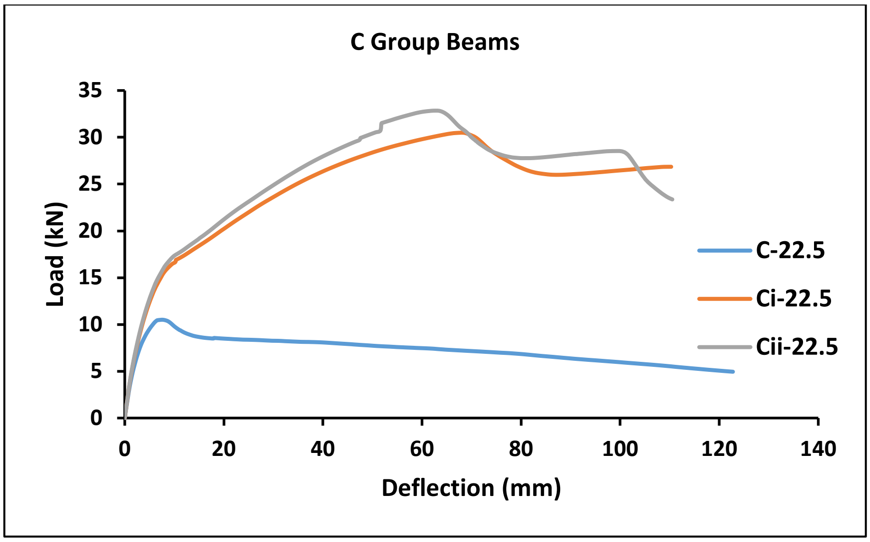

Figure 11. Load–Deflection curves of group C beams

When considered together, the load-displacement curves of the A, B, and C groups summarized in Table 10 show a consistent increase in initial stiffness, load-carrying capacity, and ductility with increasing strengthening level in all classes of concrete. The unstrengthened beams of the 10.5, 18.5, and 22.5 MPa groups achieved peak loads (Pmax) of 6.23 kN, 9.80 kN, and 10.50 kN, respectively, with relatively low stiffness and an early post-cracking degradation.

Substantial gains are seen in the beams strengthened with a single TRM + polyurea layer; for example, the peak load rises from 6.23 kN to 18.56 kN (+198%) in the 10.5 MPa group, from 9.80 kN to 29.18 kN (+198%) in the 18.5 MPa group, and from 10.50 kN to 30.47 kN (+190%) in the 22.5 MPa group - maximum deflections also increase dramatically - for instance from 8.26 mm to 51.37 mm in the lowest-strength group indicating improved ductility and stable post-cracking behavior.

The highest overall performance in each concrete class is achieved by beams strengthened with two TRM + polyurea layers. Their peak loads are equal to or exceed those values. For instance, the load at failure was increased to an impressive value of 20.55 kN (+230%) for a strength of concrete equal to f'c=10.5 MPa; similarly significant increases were observed for f'c=18.5 MPa and f'c=22.5 MPa, where Pmax was recorded as equal to or greater than values of 31.16 kN (+218%) and 32.85 kN (+213%). Further enhancements included keeping cracks nearer the surface, with narrowing plastic hinge zones, allowing softening under load to develop more gradually. This resulted in significant increases in energy dissipation capacity, from 0.569 kNm in the unstrengthened beam at f'c = 10.5 MPa to 1.81 kNm for two TRM + polyurea layers (+218%). Similar trends can also be observed for other concrete strengths.

Table 10. Structural Performance Summary of Beam Models

Concrete Strength	Model Group	Pcr (kN)	Py (kN)	Pmax (kN)	Δmax (mm)	Energy Dissipation (kN·m)
10.5 MPa	A	1.868	4.671	6.228	8.259	0.569
	Ai	5.567	13.917	18.555	51.372	1.605
	Aii	6.165	15.412	20.549	51.900	1.811
18.5 MPa	B	2.941	7.353	9.803	8.417	0.897
	Bi	8.754	21.885	29.18	74.766	2.543
	Bii	9.347	23.367	31.156	68.680	2.714
22.5 MPa	C	3.151	7.877	10.503	7.426	0.885
	Ci	9.140	22.851	30.468	67.024	2.716
	Cii	9.854	24.636	32.848	62.978	2.853

Where;

Pcr: Cracking load, Py: Yield load, Pmax: Peak load, Δmax: Deflection at peak.

6. Conclusion

In this paper, the flexural performance of hybrid TRM–polyurea–strengthened RC beams was assessed using the finite element method. Nine beam models were created based on three different concrete strength classes and three strengthening configurations. The analysis focused on the effects of the hybrid strengthening system on controlling cracks, increasing stiffness, load-carrying capacity, and ductility.

The numerical results demonstrate that the hybrid strengthening system provides a significant performance enhancement across all concrete strength levels. In the unstrengthened beams, cracks formed at early load stages, the plastic hinge region spread over a wide zone, and the load-carrying capacity remained limited despite the increase in concrete strength. In the beams strengthened with a single layer of TRM + polyurea, cracks were confined to smaller openings near the surface, the initial stiffness increased, and the peak load rose to nearly three times that of the unstrengthened model. In the beams strengthened with two TRM layers, the improvement reached its highest level; cracks were restricted to micro-segments at the surface, the width of the plastic hinge zone decreased to a minimum, and the post-peak response exhibited a more stable, plateau-like softening behavior in the load–displacement curves.

Comparison of the load-displacement curves reveals that, with increasing strengthening level, the initial stiffness increases significantly, the post-cracking becomes flatter, and the ultimate load increases systematically for all concrete groups. Beams strengthened with one TRM + polyurea layer showed significant gains in strength and deformation capacity compared to the unstrengthened models; however, those strengthened with two TRM layers achieved the highest performance in all groups. This means that hybrid systems improve not only strength but also ductility and energy absorption capacity.

Examination of the deformation modes shows that the TRM layer effectively restricts crack propagation at early stages, while the polyurea coating accommodates large deformations, enabling controlled surface-level deformation. In the unstrengthened models, cracks propagated deeply across the beam height, whereas in the two-layer TRM + polyurea models, cracks were almost completely confined to the surface and the plastic hinge region narrowed substantially. This behavior demonstrates that the hybrid system simultaneously improves stiffness and crack-control performance.

The embedded and tie interface assumptions used in the model represent an upper-bound idealization in which interface-related damage mechanisms such as debonding are neglected and perfect composite action is assumed. Despite this optimistic representation, the results obtained clearly indicate that the hybrid strengthening system is highly effective, particularly in controlling cracks, achieving a greater peak load, and improving ductility.

Overall, the analyses indicate that the TRM + polyurea hybrid system provides consistent and effective improvements in beams of all concrete strength levels examined in this study. The findings show that the hybrid strengthening approach not only enhances load-carrying capacity but also improves deformation performance in a systematic manner, offering reliable behavior independent of concrete strength. These results demonstrate that combining the crack-limiting capability of TRM with the high elongation capacity of polyurea can lead to substantial improvements in the flexural performance of reinforced concrete beams, highlighting the strong potential of the hybrid strengthening system for practical applications.

7. Future work

This numerical study has demonstrated the ability of polyurea-coated glass textile-reinforced mortar to enhance the strength of reinforced concrete beams. However, complete experimental validation studies are necessary for a safe and reliable field application of this hybrid strengthening system. Future work should include full-scale beam tests with different span lengths and load conditions to check the validity of the numerical model. Pull-off and bond-slip tests must be conducted to characterize the actual bond behavior at concrete-TRM and TRM-polyurea interfaces. More realistic interface models should be used as cohesive zone modeling instead of the perfect bond assumption currently adopted.

Additionally, extended parametric studies on polyurea thickness, the number of TRM layers, the type of textile, the strength of concrete, and behavior under cyclic loading, along with seismic effects, should be conducted. These studies should also include long-term durability and environmental exposure tests (such as moisture, temperature, and UV radiation), fire resistance assessments, and cost-benefit analyses. Finally, the applicability of this hybrid system to other structural members, such as columns or beam-slab systems, as well as its potential for shear strengthening, should be explored. Simplified design guidelines, along with application protocols for practical engineering applications, also need to be developed.

Declaration of Conflict of Interests

The authors declare that there is no conflict of interest. They have no known competing financial interests or personal relationships that could have appeared to influence the work reported in this paper.

References

[1.] Iskhakov I, Yehuda S, Ribakov Y. Modern Requirements for Strengthening and Upgrading Existing Buildings in Seismic Zones. Journal of Legal Affairs and Dispute Resolution in Engineering and Construction. 2025;17(3):04525028.

[2.] Gkournelos, P., Triantafillou, T., Bournas, D., Seismic upgrading of existing reinforced concrete buildings: A state-of-the-art review. Engineering Structures 240 (2021) 112273.

[3.] Ferrara, G., Caggegi, C., Gabor, A., Martinelli, E., Experimental study on the adhesion of basalt textile reinforced mortars (TRM) to clay brick masonry: the influence of textile density. Fibers 7 (2019) 103.

[4.] Koutas, L.N., Tetta, Z., Bournas, D.A., Triantafillou, T.C., Strengthening of concrete structures with textile reinforced mortars: State-of-the-art review. Journal of Composites for Construction 23 (2019) 03118001.

[5.] Zhou, F., Liu, H., Du, Y., Liu, L., Zhu, D., Pan, W., Uniaxial tensile behavior of carbon textile reinforced mortar. Materials 12 (2019) 374.

[6.] Kim, H.-S., Truong, G.T., Park, S.-H., Choi, K.-K., Tensile properties of carbon fiber-textile reinforced mortar (TRM) characterized by different anchorage methods. International Journal of Concrete Structures and Materials 12 (2018) 73.

[7.] De Felice, G., D'Antino, T., De Santis, S., Meriggi, P., Roscini, F., Lessons learned on the tensile and bond behavior of fabric reinforced cementitious matrix (FRCM) composites. Frontiers in Built Environment 6 (2020) 5.

[8.] Raoof, S.M., Koutas, L.N., Bournas, D.A., Bond between textile-reinforced mortar (TRM) and concrete substrates: Experimental investigation. Composites Part B: Engineering 98 (2016) 350–361.

[9.] D'Ambrisi, A., Focacci, F., Flexural strengthening of RC beams with cement-based composites. Journal of Composites for Construction 15 (2011) 707–720.

[10.] Ombres, L., Flexural analysis of reinforced concrete beams strengthened with a cement based high strength composite material. Composite Structures 94 (2011) 143–155.

[11.] Elsanadedy, H.M., Almusallam, T.H., Alsayed, S.H., Al-Salloum, Y.A., Flexural strengthening of RC beams using textile reinforced mortar–Experimental and numerical study. Composite Structures 97 (2013) 40–55.

[12.] Raoof, S.M., Koutas, L.N., Bournas, D.A., Textile-reinforced mortar (TRM) versus fibre-reinforced polymers (FRP) in flexural strengthening of RC beams. Construction and Building Materials 151 (2017) 279–291.

[13.] Park, J., Park, S.-K., Hong, S., Experimental study of flexural behavior of reinforced concrete beam strengthened with prestressed textile-reinforced mortar. Materials 13 (2020) 1137.

[14.] Giese, A.C.H., Giese, D.N., Dutra, V.F.P., Da Silva Filho, L.C.P., Flexural behavior of reinforced concrete beams strengthened with textile reinforced mortar. Journal of Building Engineering 33 (2021) 101873.

[15.] Al-Saidy, A., El-Gamal, S., Abu Sohail, K., Strengthening of reinforced concrete (RC) beams using textile reinforced mortars (TRMs). International Journal of Civil Engineering 21 (2023) 2023–2035.

[16.] Kirthiga, R., Elavenil, S., Performance evaluation of pre-damaged reinforced concrete beams strengthened with knitted glass fabric reinforced cementitious matrix: Flexure and shear behaviors. Structures 70 (2024) 107744.

[17.] Greene, C.E., Myers, J.J., Flexural and shear behavior of reinforced concrete members strengthened with a discrete fiber-reinforced polyurea system. Journal of Composites for Construction 17 (2013) 108–116.

[18.] Marawan, A., Debaiky, A., Khalil, N., Shear and flexural behavior of RC beams strengthened with polyurea spray. International Journal of Advance Research in Science and Engineering 4 (2015) 12–26.

[19.] Parniani, S., Toutanji, H., Monotonic and fatigue performance of RC beams strengthened with a polyurea coating system. Construction and Building Materials 101 (2015) 22–29.

[20.] Song, J.-H., Eun, H.-C., Improvement of flexural and shear strength of RC beam reinforced by glass fiber-reinforced polyurea (GFRPU). Civil Engineering Journal 7 (2021) 407–418.

[21.] Yu, P., Silva, P., Nanni, A., Flexural strengthening of RC beams using GFRP grid bonded with sprayed polyurea. Engineering Structures 292 (2023) 116516.

[22.] American Concrete Institute, ACI 318 – Building Code Requirements for Structural Concrete.

[23.] Lee, J., Fenves, G.L., Plastic-damage model for cyclic loading of concrete structures. Journal of Engineering Mechanics 124 (1998) 892–900.

[24.] Jankowiak, T., Lodygowski, T., Identification of parameters of concrete damage plasticity constitutive model. Foundations of Civil and Environmental Engineering 6 (2005) 53–69.

[25.] Carreira, D.J., Chu, K.-H., Stress-strain relationship for plain concrete in compression. Journal Proceedings 82 (1985) 797–804.

[26.] Turkish Standards Institution, TS 708 – Reinforcing Steel for Reinforced Concrete.

[27.] Jones, R.M., Mechanics of Composite Materials. CRC Press (2018).

[28.] Ferrara, G., Caggegi, C., Gabor, A., Martinelli, E., Experimental study on the adhesion of basalt textile reinforced mortars (TRM) to clay brick masonry: the influence of textile density. Fibers 7 (2019) 103.

[29.] Obaidat YT, Heyden S, Dahlblom O. The effect of CFRP and CFRP/concrete interface models when modelling retrofitted RC beams with FEM. Composite Structures. 2010; 92:1391–1398.

[30.] Smith-Pardo, J.P., Aristizabal-Ochoa, J.D., Second-order axial force and midspan deflection in a simple supported beam axially restrained. Engineering Structures 30 (2008) 561–569.

How to Cite This Article

Simsek, B., Arslan, A., Numerical Investigation of the Flexural Behavior of RC Beams Strengthened with Polyurea Coated Glass Textile Reinforced Mortar, Civil Engineering Beyond Limits, 1 (2026), 11094.
https://doi.org/10.36937/cebel.2026.11094